



HAL
open science

Quantitative MRI of Gd-DOTA Accumulation in the Mouse Brain After Intraperitoneal Administration: Validation by Mass Spectrometry

Anthony Tessier, Anthony Ruze, Isabelle Varlet, Estelle M.H. Laïb, Emilien Royer, Monique Bernard, Angèle Viola, Teodora-adriana Perles-barbacaru

► To cite this version:

Anthony Tessier, Anthony Ruze, Isabelle Varlet, Estelle M.H. Laïb, Emilien Royer, et al.. Quantitative MRI of Gd-DOTA Accumulation in the Mouse Brain After Intraperitoneal Administration: Validation by Mass Spectrometry. *Journal of Magnetic Resonance Imaging*, 2023, 10.1002/jmri.29034 . hal-04520141

HAL Id: hal-04520141

<https://hal.science/hal-04520141>

Submitted on 25 Mar 2024

HAL is a multi-disciplinary open access archive for the deposit and dissemination of scientific research documents, whether they are published or not. The documents may come from teaching and research institutions in France or abroad, or from public or private research centers.

L'archive ouverte pluridisciplinaire **HAL**, est destinée au dépôt et à la diffusion de documents scientifiques de niveau recherche, publiés ou non, émanant des établissements d'enseignement et de recherche français ou étrangers, des laboratoires publics ou privés.



Distributed under a Creative Commons Attribution 4.0 International License

Quantitative MRI of Gd-DOTA Accumulation in the Mouse Brain After Intraperitoneal Administration: Validation by Mass Spectrometry

Anthony Tessier, MS,^{1,2} Anthony J. Ruze, MS,¹ Isabelle Varlet, PhD,¹  Estelle M.H. Laïb, MS,¹ Emilien Royer, PhD,¹  Monique Bernard, PhD,¹  Angèle Viola, PhD,¹  and Teodora-Adriana Perles-Barbacaru, PhD^{1*} 

Background: In mice, intraperitoneal (ip) contrast agent (CA) administration is convenient for mapping microvascular parameters over a long-time window. However, continuous quantitative MRI of CA accumulation in brain over hours is still missing.

Purpose: To validate a quantitative time-resolved MRI technique for mapping the CA kinetics in brain upon ip administration.

Study Type: Prospective, animal model.

Specimen: 25 C57Bl/6JRj mice underwent MRI.

Field Strength/Sequence: 7-T, gradient echo sequence.

Assessment: Gd-DOTA concentration was monitored by MRI (25 s/repetition) over 135 minutes with (N = 15) and without (N = 10) ip mannitol challenge (5 g/kg). After the final repetition, the brains were sampled to quantify gadolinium by mass spectrometry (MS). Upon manual brain segmentation, the average gadolinium concentration was compared with the MS quantification in transcardially perfused (N = 20) and unperfused (N = 5) mice. Precontrast T₁-maps were acquired in 8 of 25 mice.

Statistical Tests: One-tailed Spearman and Pearson correlation between gadolinium quantification by MRI and by MS, D'Agostino-Pearson test for normal distribution, Bland-Altman analysis to evaluate the agreement between MRI and MS. Significance was set at *P*-value <0.05.

Results: MRI showed that ip administered CA reached the blood compartment (>5 mM) within 10 minutes and accumulated continuously for 2 hours in cerebrospinal fluid (>1 mM) and in brain tissue. The MRI-derived concentration maps showed interindividual differences in CA accumulation (from 0.47 to 0.81 mM at 2 hours) with a consistent distribution resembling the pathways of the glymphatic system. The average in-vivo brain concentration 2 hours post-CA administration correlated significantly (*r* = 0.8206) with the brain gadolinium quantification by MS for N = 21 paired observations available.

Data Conclusion: The presented experimental and imaging protocol may be convenient for monitoring the spatiotemporal pattern of CA uptake and clearance in the mouse brain over 2 hours. The quantification of the CA from the MRI signal in brain is corroborated by MS.

Evidence Level: N/A

Technical Efficacy: Stage 1

J. MAGN. RESON. IMAGING 2023.

View this article online at wileyonlinelibrary.com. DOI: 10.1002/jmri.29034

Received Jul 4, 2023, Accepted for publication Sep 19, 2023.

*Address reprint requests to: T.-A.P.-B., CRMBM UMR CNRS 7339, Faculté des Sciences Paramédicales et Médicales La Timone, Aix-Marseille Université, 27, bd. Jean Moulin, 13005 Marseille, France.
E-mail: teodora.perles-barbacaru@univ-amu.fr

From the ¹CNRS, Center for Magnetic Resonance Imaging in Biology and Medicine (CRMBM, UMR CNRS 7339), Aix-Marseille University, Marseille, France; and ²Department of Medical Imaging, Sainte-Anne Military Teaching Hospital (Hôpital d'Instruction des Armées), Toulon, France

Additional supporting information may be found in the online version of this article

This is an open access article under the terms of the [Creative Commons Attribution](https://creativecommons.org/licenses/by/4.0/) License, which permits use, distribution and reproduction in any medium, provided the original work is properly cited.

Microvascular changes accompany normal brain development¹ and aging,² but also various neurodegenerative, neuroinflammatory, neoplastic, psychiatric, and metabolic pathologies.^{3–6} Vascular involvement has been established in animal models of Alzheimer's disease,⁷ epilepsy,⁸ depression,⁹ cerebral malaria,¹⁰ amyotrophic lateral sclerosis,¹¹ and multiple sclerosis.¹² Robust and noninvasive quantification of microvascular parameters, such as the cerebral blood volume (CBV), cerebral blood flow, and altered endothelial permeability is required for the early detection, characterization, and therapeutic follow-up of such diseases. Although MRI methods such as arterial spin labeling and diffusion weighted approaches exploiting endogenous contrast mechanisms are under development,^{13,14} most MRI approaches such as dynamic contrast enhanced (DCE), dynamic susceptibility contrast and steady state contrast enhanced techniques still rely on intravenously (iv) administered contrast agents (CA). The efflux of metabolic waste products from the interstitial fluid involves perivascular and perineural pathways constituting the glymphatic system, with waste ending up in the subarachnoid space and draining into meningeal and nasal lymphatic vessels and cervical lymph nodes.¹⁵ Like the vascular system, the glymphatic system can be impaired in neurodegenerative diseases, including Alzheimer's disease and cerebral small vessel disease.¹⁶ Recently, DCE-like MRI protocols based on intrathecal or intracisternal CA administration have been proposed to study the pathways of the glymphatic system in rodents.^{17,18} These protocols require the quantification of the CA in tissue from T₁-weighted dynamic MRI,¹⁹ which is not straightforward because it requires acquisition of a proton density (PD) or T₁ weighted acquisition before CA administration for reference, a quasi-linear or otherwise known relationship between the signal and CA concentration over a wide range, minimization of confounding effects from flow and T₂(*) changes as well as whole brain coverage with a reasonable time resolution. Alternatively, pre- and post-contrast T₁ relaxometry can be used but is generally more time consuming.

A time resolved MRI approach has been proposed to monitor CA uptake into the brain parenchyma upon intravenous²⁰ and intraperitoneal (ip) administration.²¹ So far, this approach has only been used to quantify the regional CBV and CBV changes upon a pharmacological challenge,²¹ similarly to iron oxide particle-based pharmacological MRI approaches.²² However, similarly to DCE-MRI, it allows to detect accumulation of the CA beyond the vascular compartment.²³ Such CA accumulation can either be triggered by a drug or a functional change or because of a pathology affecting the endothelial permeability^{20,23} or the efficacy of the glymphatic efflux. This approach does not yield quantitative parameters for the blood flow and the endothelial permeability. However, its easy implementation is of interest in mouse models characterized by a slow accumulation of the CA

and/or an impaired clearance since the regional CA uptake rate is appropriate to characterize the tissue, disease induced changes, or pharmacological effects. In many applications, the aim is to detect if and when the CA accumulates in the brain tissue.

Against this background, we aimed to validate this time resolved MRI approach for the quantitative assessment of the CA concentration, and to investigate the spatiotemporal distribution in mouse brain upon its ip administration. We also employed this approach to detect if the CA accumulates in brain tissue upon pharmacological challenge with ip hyperosmolar mannitol.

Materials and Methods

This pilot study was carried out in accordance with French regulations (decree 2013-118) and the European directive (2010/63/EU) on the protection of animals used for scientific purposes after approval by our institutional committee on ethics and the ministry of higher education and research (project authorization #31714).

Animals and Experimental Procedure

Female 14- to 16-week-old C57Bl/6J mice (N = 25; Janvier Labs, Le Genest-Saint-Isle, France), weighing 21.6 ± 1.6 g and housed in groups in an enriched specific pathogen-free environment with food and water ad libitum, were randomly allocated to one of two groups (group 1: control N = 10; group 2: mannitol N = 15) by a zoo-technician unaware of the study design. Further blinding was impractical since the researchers were involved in all experimental and analysis procedures. The study was carried out during the light phase of the 12-hour light/dark cycle. Catheterization of the peritoneal cavity with two 24G catheters and MRI acquisitions were performed under isoflurane (1.5%–2%/air; Vetflurane, Virbac, Centravet, Lapalisse, France). The mouse eyes were lubricated (Ocry-gel, Tvm laboratory, Lempdes, France). In the magnet, rectal temperature (35–37°C) and respiration (80–120 minutes⁻¹) were monitored continuously.

During dynamic MRI acquisition, the low-molecular-weight (0.5 kDa) macrocyclic-gadolinium-chelate Gd-DOTA (Dotarem® 0.5 M; Guerbet, Villepinte, France) was administered ip at 10 mmol/kg^{21,24} via the prefilled extension line. The second line was used 15 minutes later to administer isotonic saline solution (B. Braun, Saint-Cloud, France; group 1) or 5 g/kg of 20% mannitol solution (Macopharma, Mauvaux, France) to increase the Gd-DOTA uptake (group 2). The warmed solutions were injected over 2 minutes, limiting temperature decrease and cardiorespiratory effects. At the end of the protocol, isoflurane was increased to 5% to ensure deep anesthesia (respiration rate < 20 minutes⁻¹).

In 20 mice (10 from group 1 and 10 mannitol-treated mice from group 2), the CA was removed from the blood pool by transcardial perfusion (Supplementary Materials and Methods). The unperfused mice (5 mannitol-treated mice from group 2) were euthanized by cervical dislocation, the brains were extracted, freeze-clamped in liquid nitrogen, and stored at -80°C. The delay between the last MRI acquisition and the interruption of the blood flow by cervical dislocation or perfusion was approximately 2 and 10 minutes, respectively.

TABLE 1. MRI Acquisition Parameters

Acquisition	T ₁ Map	MRA	PD	trMRI	T ₁ w
Sequence	RARE-VTR	2D-FLASH	3D-FLASH	3D-IR-FLASH	3D-IR-FLASH
FOV (mm ³)	15 × 15 × 0.5	15 × 15 × 16.5	15 × 15 × 16.5	15 × 15 × 16.5	15 × 15 × 16.5
Matrix	64 × 64 × 1	64 × 64 × 33	64 × 64 × 33	64 × 64 × 33	200 × 200 × 33
Voxel size (μm ³)	234 × 234 × 500	234 × 234 × 500	234 × 234 × 500	234 × 234 × 500	75 × 75 × 500
TR/TE (msec)	15,000, 6000, 3000, 1500, 750/6	4.4/1.2	25,000/1.5	750/1.5	3000/1.8
TI/TR _{echo} (msec)	–/–	–/–	–/5	295/5	1050/9.5
Flip angle (°)	90	80	10	180/10	180/15
Acceleration	Factor 2				
NA/NR	1/1	2/1	1/1	1/300 + 20	1/1
Duration	12 minutes 56 seconds	15 seconds	13 minutes 45 seconds	123 + 8 minutes	5 minutes 33 seconds
Purpose	Confirmation of representative cerebral T ₁₀ value	Control of the absence of motion	Thermal equilibrium signal for normalization	Detection of CA accumulation	Anatomical details

CA = contrast agent; MRA = MR angiography; PD = proton density; trMRI = time resolved MRI; RARE = rapid acquisition with relaxation enhancement spin echo; VTR = variable repetition time; FLASH = fast low angle shot gradient echo; FOV = field of view; TE = echo time; TI = inversion time; TR_{echo} = inter echo repetition time; NA = number of averages; NR = number of repetitions; T₁₀ = longitudinal relaxation time constant prior to CA administration. For all sequences, TE was minimized.

MRI Protocol

Brain exploration was performed on a 7-T preclinical MRI scanner (PharmaScan 70/16 US; Bruker, Wissembourg, France) equipped with 760 mT/m magnetic field gradients (BGA 9S HP), a volume resonator (diameter of 72 mm) for emission, a 2 × 2 elements cryogenic mouse head surface coil for reception, and ParaVision 6.0 software (Bruker, Wissembourg, France).

The mice were positioned prone. All images were acquired in the axial plane and covered the entire brain from the olfactory bulbs to the cerebellum, except for single-slice T₁ maps, which were acquired at bregma level. Field homogeneity was accomplished using a B₀ map shim technique.

Before Gd-DOTA administration, the imaging protocol (Table 1; Fig. 1) consisted of a brief angiography, and in a

subset of 8 mice of five T₁-weighted images to compute T₁ maps. The MRI technique used to map the CBV and the Gd-DOTA uptake required an acquisition at thermodynamic equilibrium (termed PD) to normalize the time resolved T₁-weighted signal (trMRI), which was acquired with an inversion recovery-prepared fast gradient echo with experimentally optimized parameters (Table 1) to suppress the signal from the brain parenchyma and the blood prior to Gd-DOTA injection.²¹ A baseline signal was acquired over 5 minutes before Gd-DOTA injection. The trMRI signal was then acquired over 135 minutes interrupted once at 120 minutes by a second angiography to confirm the absence of motion by superposition onto the precontrast angiography and by a T₁-weighted high-resolution image for anatomical reference.

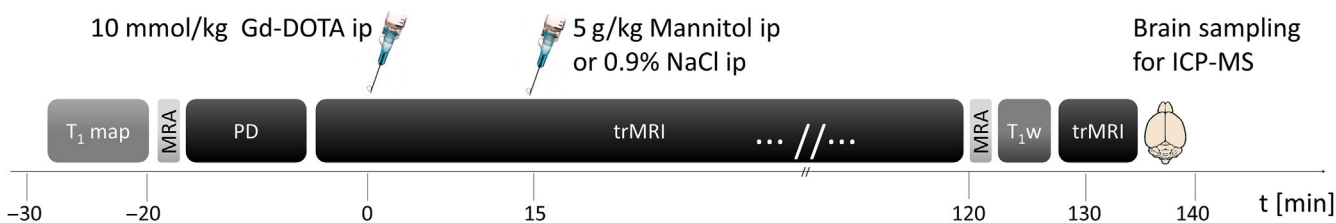


FIGURE 1: Timeline of the MRI acquisition protocol taking approximately 2 hours 40 minutes per animal. The time point of Gd-DOTA administration during the time resolved MRI acquisition was set to zero. MRA = MR angiography; PD = proton density; trMRI = time resolved MRI.

Mass Spectroscopy

The frozen brain samples were desiccated and prepared for gadolinium quantification by inductively coupled plasma mass spectrometry (ICP-MS model 7800, Agilent Technologies, Les Ulis, France). Methodological details are provided in the Supplementary Materials and Methods).

The gadolinium concentration was converted from $\mu\text{g}\cdot\text{g}^{-1}$ dry tissue to millimolar (mM) using a dilution factor of 1/5 upon desiccation and a brain density of 1046 g L^{-1} .²⁵

Data Processing

All MRI processing and analysis were performed under ImageJ (version 1.53; <https://imagej.nih.gov/ij/>) on 32bit_FLOAT reconstructed images. Quantitative T_1 maps were calculated using Eq. 1 (Table 2).

Based on simplifying assumptions generally made for DCE-MRI (and detailed in Supplementary Materials and Methods), the trMRI signal $S(t)$ can be analyzed using Eq. 2 (Table 2).²⁰ Eq. 2 represents the distribution volume fraction (DVF) as long as the CA is confined to a tissue compartment at a concentration above $C_{\text{crit}} = 5\text{ mM}$. At this concentration, the short T_1 of this compartment allows its signal to reach the thermodynamic equilibrium while the signal from compartments with long T_1 is negligible. The tissue signal is therefore proportional to the volume fraction of the distribution compartment. A constant trMRI signal shortly after CA arrival in the brain tissue is known to arise from the vascular compartment.^{20,21}

Contrary to previous studies aiming at the quantification of the DVf of the CA,^{20,21,23} we did not assume that the C_{crit} was attained or maintained over the entire observation time. Instead, the normalized trMRI signal was converted into longitudinal relaxation rate R_1 ²⁶ (Fig. S1a), from which regional CA concentration was estimated (Eqs. 3 and 4, Table 2). The normalized trMRI signal is almost linearly dependent on CA concentration for $1.18 < R_1 < 10\text{ second}^{-1}$ (or $850 > T_1 > 100\text{ msec}$), corresponding to tissue concentrations of $0.16 < C < 2.7\text{ mM}$ (Fig. S1a).

A vascular concentration $> C_{\text{crit}}$ is necessary to quantify the cerebral blood volume fraction (BVf), yet the signal is saturated leading to an underestimation of the CA concentration in tissue while it is confined to the vascular space (Fig. S1b). The trMRI signal might decrease again, reflecting a CA concentration decrease below C_{crit} .

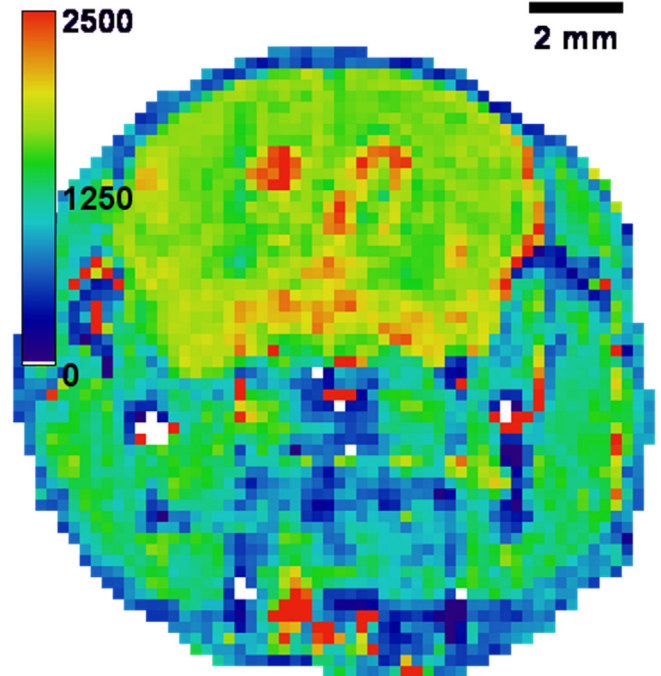


FIGURE 2: Representative axial T_1 map in milliseconds of mouse brain tissue in-vivo at 7-T. The white pixels represent failed fit.

However, any observed trMRI signal increase arises from CA accumulation within the extravascular compartment (Fig. S1b),²³ even if the vascular CA concentration does not remain above C_{crit} over the entire observation interval.

The conversion depends on the tissue relaxivity of Gd-DOTA assumed to be in the interval $2.8\text{ mM}^{-1}\text{ s}^{-1} \leq r_1 \leq 3.6\text{ mM}^{-1}\text{ s}^{-1}$ for whole blood²⁷ and plasma²⁸ at 7-T and 37°C and on the baseline relaxation rate R_{10} ($= T_{10}^{-1}$) of brain tissue. To avoid lengthy acquisitions of T_1 maps for each mouse, Gd-DOTA concentration maps were computed using an average R_{10} of 0.6 second^{-1} . Concentration maps were generated by averaging 20 trMRI repetitions up to 15 minutes and up to 135 minutes after Gd-DOTA administration, when available, otherwise up to the last trMRI time point. The brain tissue was delineated manually (by ATPB, 19 years of experience in rodent models) on each slice of the PD acquisition

TABLE 2. Analysis of MRI Acquisitions

Parameter of Interest	Relation	Equation	Reference
Longitudinal relaxation rate prior to CA administration R_{10}	$S(TR) = S_0 [1 - \exp(-TR \cdot R_{10})]$	1	37
Normalized signal intensity $\frac{M_z}{M_0}$	$\frac{M_z(t)}{M_0} = \frac{S(t) - S_{\text{preCA}}}{S_0}$	2	Eq. 1 in Ref. ²¹
Longitudinal relaxation rate R_1	$\frac{M_z}{M_0}(R_1) = 1 - \frac{2 \exp(-TI \cdot R_1)}{1 + \exp(-TR \cdot R_1)}$	3	Eq. 7 in Ref. ²⁶
Tissue concentration C	$C(t) = \frac{R_1(t) - R_{10}}{r_1}$	4	38

CA = contrast agent; S = T_1 -weighted signal; S_0 = proton density signal; TR = repetition time; M_z = T_1 -weighted longitudinal magnetization; M_0 = thermal equilibrium magnetization; S_{preCA} = baseline dynamic MRI signal prior to CA administration; TI = inversion time; R_{10} = longitudinal relaxation rate prior to contrast agent administration; r_1 = longitudinal contrast agent relaxivity.

(Fig. S2), taking care to only include structures collected for ICP-MS. Extracerebral cerebrospinal fluid (CSF), cranial nerves, and the pituitary gland were therefore excluded. The Gd-DOTA concentration was then averaged within the delineated brain mask (16480 ± 708 voxels). The ventricles were also segmented (by IV, 8 years of experience in brain segmentation, 407 ± 148 voxels). Maximum intensity projections were generated from the 3D MRI volumes after segmentation of the brain.

Statistical Analysis

Analysis was performed with Prism software (version 9.0; GraphPad Software, San Diego, CA, USA). The measured parameters were the MRI estimate of the Gd-DOTA concentration averaged over the entire brain at the end of the observation interval and the quantification of gadolinium by ICP-MS. Bland–Altman, one-tailed Spearman correlation, D’Agostino–Pearson test for normal distribution, and Pearson correlation analyses were performed. Values were

expressed as mean \pm standard deviation. A P -value <0.05 was considered statistically significant.

Results

The average T_{10} for intraventricular CSF and brain tissue was 2.266 ± 0.222 seconds and 1.625 ± 0.039 seconds, respectively ($N = 8$), i.e. $T_{10} > 1$ second as necessary for signal suppression prior to CA administration (Fig. 2).

From the constant trMRI signal observed in brain tissue in the 10–15 minutes interval after CA administration an average BVf in the order of 0.02 was measured.

The Gd-DOTA concentration in brain tissue was in the order of 0.2 mM 15 minutes after CA administration. Two hours later, it reached 0.5 mM on average in brain tissue and above 1 mM in CSF. This CA concentration range falls within the fairly linear part of the signal to concentration dependence (Fig. S1a).

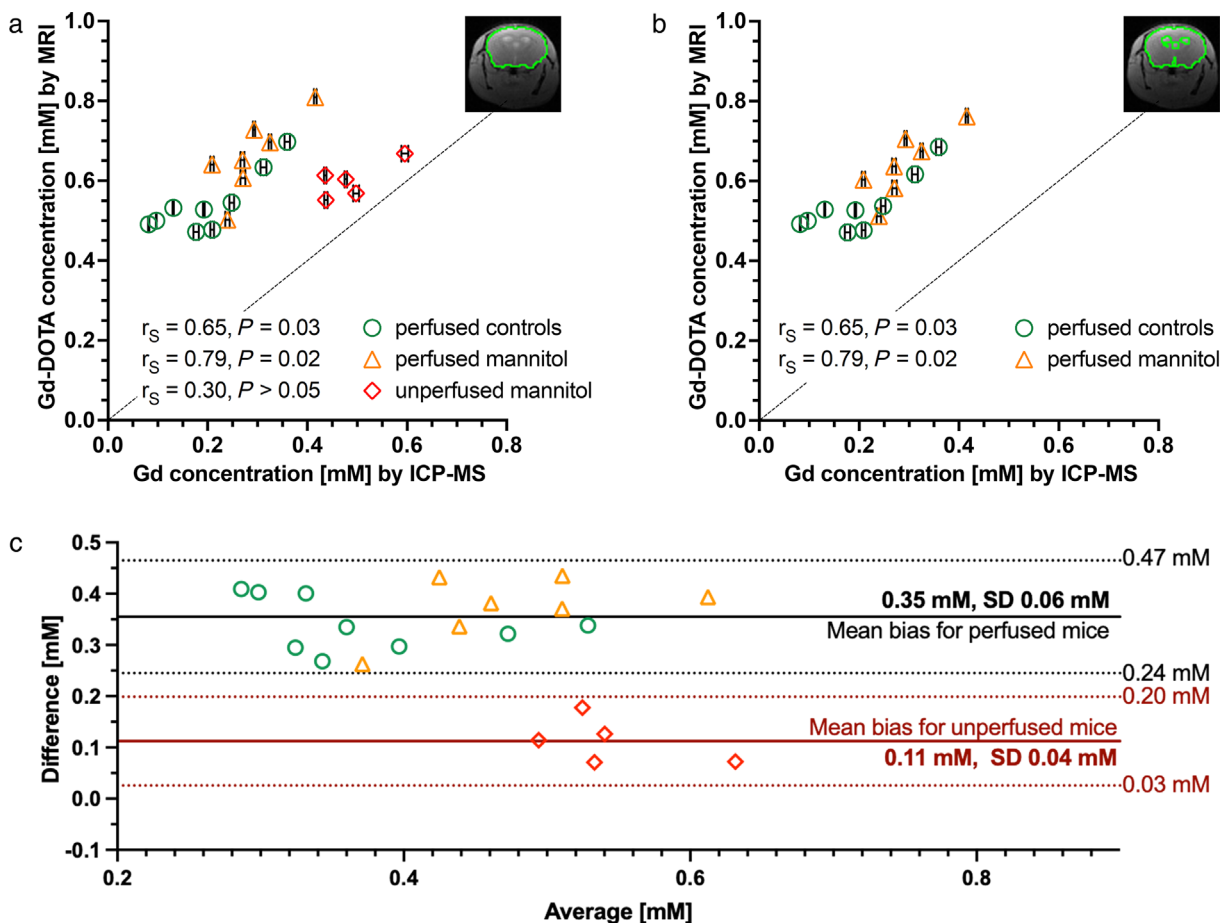


FIGURE 3: Comparison between in-vivo Gd-DOTA estimation by MRI and ex-vivo gadolinium quantification by ICP-MS. For correlation analysis, the MRI measures were made in brain tissue including (a) and excluding (b) the ventricular CSF. The correlation coefficients remained unchanged when excluding the ventricles. The result of nonparametric correlation is shown because the two groups of perfused mice ($N = 7$) and unperfused mice ($N = 5$) treated with mannitol did not pass the normality test. When grouping all data for perfused mice regardless of treatment ($N = 16$), the correlation was significant (Spearman $r = 0.8206$, Pearson $r = 0.8407$, $P < 0.001$ for both). The gadolinium concentration by ICP-MS obtained on unperfused brains was close to the line of identity. The error bars show the standard deviation (SD) of the ICP-MS measures for four gadolinium isotopes. The MRI measures have no error bars because averaging over all brain regions produced standard deviations too high and standard errors too small to be displayed. (c) Bland–Altman plot showing bias and 95% limits of agreement separately for perfused mice (0.35 mM, 0.24 to 0.47 mM, $N = 16$) and for unperfused mice (0.11 mM, 0.03 to 0.20 mM, $N = 5$). An r_1 of $3.6 \text{ mM}^{-1} \text{ s}^{-1}$ was used for conversion of the trMRI signal.

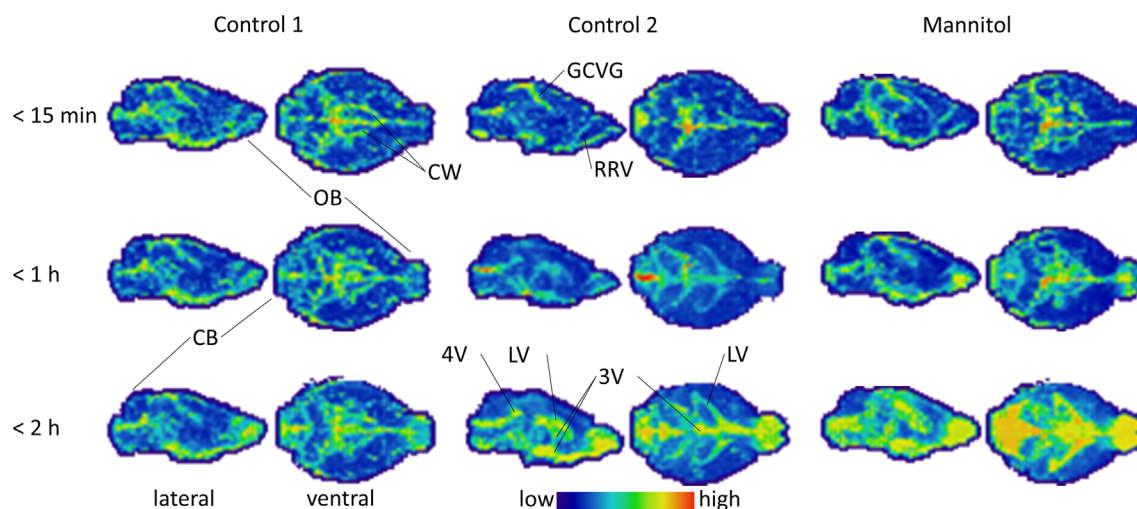


FIGURE 4: Spatiotemporal distribution of Gd-DOTA accumulation in brain tissue and ventricular CSF. Maximum intensity projections (lateral and ventral views) generated from the 4D concentration maps show the spatial distribution of the contrast agent at three time points of the observation interval for two control mice and one mannitol treated mouse showing different degrees of uptake. OB = olfactory bulb; CW = circle of Willis; CB = cerebellum; GCVG = great cerebral vein of Galen; RRV = rostral rhinal vein; LV = lateral ventricles; 3V = 3rd ventricle; 4V = 4th ventricle. The nine corresponding animated gif files are available as supplementary figures (Figure S3).

With three exceptions, mannitol-treated mice showed signs of cardiorespiratory failure before the intended end of the trMRI acquisition, in which case the acquisition was interrupted, the animal euthanized, the brain processed as planned and data included in the analysis. Due to motion artifacts ($N = 2$), failed MRI acquisition ($N = 1$), and failed ICP-MS quantification ($N = 1$), both measures were only available for 16 perfused and 5 unperfused mice (Fig. 3). Our study showed no evidence of Gd-DOTA loss from the ventricular CSF due to transcerebral perfusion or brain sampling (Fig. 3b). Despite a significant correlation (Fig. 3; Table S1), the MRI-derived concentration was noticeably higher since it included the CA in the blood pool. This is reflected by the bias of 0.35 mM in the Bland–Altman analysis (Fig. 3c). For unperfused mice, the two techniques yielded more comparable values, in particular for $r_1 = 3.6 \text{ mM}^{-1} \text{ s}^{-1}$. An r_1 of $2.8 \text{ mM}^{-1} \text{ s}^{-1}$ would result in MRI measures that are a factor of $3.6/2.8 = 1.2857$ higher.

Immediately after injection, Gd-DOTA was mainly seen in the vascular system (Fig. 4). Furthermore, Gd-DOTA accumulation occurred in ventricular CSF within the first hour and in periventricular parenchyma, particularly in the hypothalamus, beyond 1 hour after administration. The Gd-DOTA uptake was also predominant in the olfactory bulb. The spatiotemporal CA accumulation pattern was similar for all mice, though with variable degree of accumulation among mice (Figs. 3 and 4). Mannitol treatment, despite the relatively low dose, increased tissue uptake of Gd-DOTA in 11/12 mice.

Discussion

This study shows that, in addition to the quantification of the regional cerebral BVf, the proposed trMRI approach is

able to detect CA accumulation over time and to monitor its uptake kinetics in a quantitative and direct way. The approach is suited for the detection of vasoactive or blood–brain barrier modulating properties of pharmacological agents, and for the study of the spatiotemporal distribution of CAs, including efflux via the glymphatic pathways.

The measured BVf of 0.02 is in agreement with previous studies using the trMRI technique with an ip Gd-DOTA dose of 6 mmol/kg at 4.7-T²¹ or other approaches,^{29,30} confirming that the quantitative measure is independent of B_0 and CA dose. Knowledge of the tissue T_1 or the vascular input function is not required to map this parameter. Only the PD acquisition was required for quantification.

The T_{10} map was only acquired for validation purposes. Due to the longer baseline T_{10} , the CA concentration estimation in ventricular CSF has the highest inaccuracy when assuming a global R_{10} of 0.6 second^{-1} . About 15 minutes after CA administration when the tissue concentration was still low, the concentration can be underestimated by up to 30% in CSF and overestimated by up to 15% in brain structures with lower T_{10} such as white matter. Two hours after administration, the high tissue CA concentration reduced the relative error to 5%.

Although individual T_{10} maps covering the entire brain may increase the accuracy of the quantification in particular for low CA concentrations, we believe that the use of a single representative T_{10} value for brain tissue is acceptable for most preclinical studies allowing to save overall acquisition time or to lengthen the observation time of the trMRI acquisition to ensure the desired pharmacological effect can be observed.

Compared to steady-state techniques such as the CA-based vascular space occupancy technique that shares the

same assumptions, the described trMRI technique has the advantages of more reliable blood nulling, and the detection of CA extravasation owing to the time resolved acquisition. This study showed that even slow and subtle CA accumulation in brain parenchyma after ip administration in control mice can be detected and quantified with the time resolved MRI approach. It can be used for pharmacological MRI when using a CBV-modifying drug or in response to hypercapnia,²⁶ or to detect disruption of the blood–brain barrier (BBB) by focused ultrasound, ischemia, intracarotid hyperosmolar mannitol administration, or death.

Specifically, ip administration routes are of interest and comparable with iv routes when using CAs such as Gd-DOTA and MnCl₂,^{24,31} albeit with a slight delay resulting from the time required for the CA to reach the vasculature. In addition to the ease of (repeated) catheterization and the less stringent restrictions on injectable volume in mice,³² ip administration resembles an iv continuous infusion due to the CA reservoir in the peritoneal cavity and lengthens the observation time window.

The ip administration route is also less invasive and less technically challenging than the intrathecal, intracisternal or intracerebroventricular administration of CA, and this study showed that it may result in a comparable spatial distribution in the brain within the same observation time. In this study, slow ip bolus injection led to a reasonable observation time. A dose of 10 mmol/kg Gd-DOTA (higher than the recommended dose of 6 mmol/kg²¹) was administered in this exploratory study involving MRI at higher magnetic field and euthanasia for brain sampling. Alternatively, an ip continuous infusion protocol can be established following a lower initial dose.

Hyperosmolar mannitol is known to increase the BBB permeability but high doses also raise the cerebral BVf.³³ Both changes lead to an increase of the tissue Gd-DOTA concentration and therefore to a trMRI signal increase. However, the correlation between in-vivo and ex-vivo measures in mannitol-treated and transcardially perfused mice would be compromised if BVf increases were the source of signal increase. The ICP-MS-based Gd quantification in perfused mice confirmed that gadolinium indeed reached the interstitial space.

The spatial distribution is evocative of the one observed in rodent studies with intracisternal or intraventricular CA or fluorescent tracer administration^{17,18} highlighting the role of the glymphatic system in the transport of the CA to the brain parenchyma, in particular under hyperosmolar conditions.³⁴

Limitations

Technical advances such as parallel imaging and sparse sampling and reconstruction techniques can improve the compromise between spatial and temporal resolution of the MRI acquisition.³⁵ As other dynamic techniques, it has a high

sensitivity to motion that is difficult to correct using image registration due to the signal nulling of brain and extracerebral tissue before CA arrival.

Time resolved MRI without pharmacokinetic modeling is not suited for the quantification of the microvascular permeability, but mapping the CA concentration over time allows estimation of a regional accumulation rate, which is generally expected to qualitatively reflect microvascular leakiness.³⁶ However, as is the case for the volume transfer constant K^{trans} , the contribution of permeability, blood flow and—with long observation times—interstitial diffusion cannot be disentangled. Despite dynamic monitoring of the MRI signal change, pharmacokinetic modeling yields a set of quantitative microvascular parameters that is not time-resolved and requires determination of the arterial input function and an appropriate compartment model, including the vascular, interstitial, and CSF space.³⁶ This study aimed at validating a direct and functional MRI technique for the mapping of the accumulation rate over hours.

While the parenchymal CA concentration was the measure ultimately aimed for, the tissue concentration of the CA mapped by MRI is a surrogate measure and the combined result of the microvascular BVf, the plasma concentration of the CA, the microvascular leakiness, and the existence of alternative routes for the CA to reach the parenchyma.^{18,34} On the one hand, in case of large CA accumulation in the interstitial fluid, signal saturation and the slow transcytolemmal water exchange regime might have led to an underestimation of the tissue concentration, as during confinement of the CA in the blood pool. On the other hand, when interstitial CA accumulation is very weak and interstitial T_1 is above 850 msec, the interstitial signal remains nulled, masking the weak accumulation. For an initial tissue relaxation rate of 0.6 second^{-1} and a relaxivity of $3.6 \text{ mM}^{-1} \text{ s}^{-1}$, $T_1 < 850 \text{ msec}$ is reached at a concentration above 0.16 mM, which constitutes the detectability limit. Below this CA concentration or for tissue $T_1 > 850 \text{ msec}$, dynamic MRI with the chosen acquisition parameters is not suitable for quantification. If required for certain applications, the detectability limit can be lowered for instance by increasing the inversion time, taking care not to compromise the suppression of the tissue and blood signal.

Quantitative comparisons between in-vivo and ex-vivo modalities are affected by methodological difficulties. Parenchymal CA accumulation is expected to have continued after the last MRI acquisition and at blood flow arrest due to tissue hypoxia.¹⁵ Brain sampling and subsequent tissue processing are prone to partial tissue loss; eg, loss of small parts of the highly CA accumulating olfactory bulb can affect the average gadolinium quantification. Manual segmentation is subjective particularly in areas affected by partial volume effects, and exact correspondence of segmented structures with actually sampled tissue is uncertain, eg, for nerve roots, CSF in lateral recesses of the 4th ventricle, and the olfactory nerve layer.

Last but not least, the tissue CA relaxivity might be $>3.6 \text{ mM}^{-1} \text{ s}^{-1}$, i.e., beyond the range of estimates inferred from in-vitro studies,^{27,28} as suggested by the comparison of MRI and ICP-MS gadolinium quantification for unperfused mice. The validation of the quantitative aspect of the trMRI approach over time would be a typical application of simultaneous PET—MRI acquisitions in conjunction with a bimodal imaging agent.

Bland–Altman analysis revealed reasonable agreement between gadolinium quantification by MRI and ICP-MS and confirmed a systematically higher value with MRI for perfused mice. Even for unperfused mice, the bias is still 0.11 mM (approximately 20% of the average gadolinium concentration). However, this analysis is limited by the small number of paired measures (a single measure per mouse, $N = 21$). Regional Gd quantification by ICP-MS has not been performed. This exploratory study revealed that the cerebral Gd-DOTA concentration is beyond the sensitivity limits of ICP-MS even in control mice, thus future studies will include quantification of the gadolinium content in sub-regions of the brain for correlation with MRI estimations. Additional studies are needed to distinguish whether CA accumulation results from extravasation or whether transport via the perivascular pathways of the glymphatic system is predominant.

Conclusion

We demonstrated that quantitative mapping of CA uptake in brain upon ip administration is feasible by time resolved MRI without pharmacokinetic modeling. The ip administered CA reaches the cerebral vasculature within 5 minutes and can be a minimally invasive alternative to iv administration. The ip administration route considerably lengthens the observation time.

Acknowledgments

We thank Laurent Vassalo and Carine Demelas from The Laboratory of Environmental Chemistry (LCE) UMR 7376, Marseille, France, for the gadolinium quantification by inductively coupled plasma mass spectrometry and helpful discussions. Centre de Calcul Intensif d’Aix-Marseille is acknowledged for granting access to its high-performance computing resources. This study has received funding by CNRS (Centre National pour la Recherche Scientifique) and Aix-Marseille University. CRMBM is a member of France Life Imaging Network (grant ANR-11-INBS-0006 from the French “Investissements d’Avenir” program). Financial support for a student fellowship (Estelle Laib) from Marseille Imaging Institute (AMX-19-IET-0023) is also acknowledged.

References

1. Harb R, Whiteus C, Freitas C, Grutzendler J. In vivo imaging of cerebral microvascular plasticity from birth to death. *J Cereb Blood Flow Metab* 2013;33:146-156.
2. Hill LK, Hoang DM, Chiriboga LA, Wisniewski T, Sadowski MJ, Wadghiri YZ. Detection of cerebrovascular loss in the normal aging C57BL/6 mouse brain using in vivo contrast-enhanced magnetic resonance angiography. *Front Aging Neurosci* 2020;12:585218.
3. Wei Z, Liu H, Lin Z, et al. Non-contrast assessment of blood-brain barrier permeability to water in mice: An arterial spin labeling study at cerebral veins. *Neuroimage* 2023;268:119870.
4. Tysiak E, Asbach P, Aktas O, et al. Beyond blood brain barrier breakdown – in vivo detection of occult neuroinflammatory foci by magnetic nanoparticles in high field MRI. *J Neuroinflammation* 2009;6:20.
5. Yoshikawa M, Aizawa S, Oppenheim RW, Milligan C. Neurovascular unit pathology is observed very early in disease progression in the mutant SOD1G93A mouse model of amyotrophic lateral sclerosis. *Exp Neurol* 2022;353:114084.
6. Cai L, Li W, Zeng R, et al. Valsartan alleviates the blood-brain barrier dysfunction in db/db diabetic mice. *Bioengineered* 2021;12:9070-9080.
7. Quintana DD, Anantula Y, Garcia JA, et al. Microvascular degeneration occurs before plaque onset and progresses with age in 3xTg AD mice. *Neurobiol Aging* 2021;105:115-128.
8. Bankstahl M, Breuer H, Leiter I, et al. Blood-brain barrier leakage during early epileptogenesis is associated with rapid remodeling of the neurovascular unit. *eNeuro* 2018;5:ENEURO.0123-18.2018.
9. Menard C, Pfau ML, Hodes GE, et al. Social stress induces neurovascular pathology promoting depression. *Nat Neurosci* 2017;20:1752-1760.
10. Penet M-F, Viola A, Confort-Gouny S, et al. Imaging experimental cerebral malaria in vivo: Significant role of ischemic brain edema. *J Neurosci* 2005;25:7352-7358.
11. Zhong Z, Deane R, Ali Z, et al. ALS-causing SOD1 mutants generate vascular changes prior to motor neuron degeneration. *Nat Neurosci* 2008;11:420-422.
12. Uchida Y, Sumiya T, Tachikawa M, et al. Involvement of Claudin-11 in disruption of blood-brain, -spinal cord, and -arachnoid barriers in multiple sclerosis. *Mol Neurobiol* 2019;56:2039-2056.
13. Kanda T, Ishii K, Kawaguchi H, Kitajima K, Takenaka D. High signal intensity in the dentate nucleus and globus pallidus on unenhanced T1-weighted MR images: Relationship with increasing cumulative dose of a gadolinium-based contrast material. *Radiology* 2014;270:834-841.
14. Marckmann P, Skov L, Rossen K, et al. Nephrogenic systemic fibrosis: Suspected causative role of gadodiamide used for contrast-enhanced magnetic resonance imaging. *J Am Soc Nephrol* 2006;17:2359-2362.
15. Ma Q, Ries M, Decker Y, et al. Rapid lymphatic efflux limits cerebrospinal fluid flow to the brain. *Acta Neuropathol* 2019;137:151-165.
16. Cannistraro RJ, Badi M, Eidelman BH, Dickson DW, Middlebrooks EH, Meschia JF. CNS small vessel disease: A clinical review. *Neurology* 2019;92:1146-1156.
17. Benveniste H, Lee H, Ozturk B, et al. Glymphatic cerebrospinal fluid and solute transport quantified by MRI and PET imaging. *Neuroscience* 2021;474:63-79.
18. Iliff JJ, Lee H, Yu M, et al. Brain-wide pathway for waste clearance captured by contrast-enhanced MRI. *J Clin Invest* 2013;123:1299-1309.
19. Buckley DL, Parker GJM. Measuring contrast agent concentration in T1-weighted dynamic contrast-enhanced MRI. In: Jackson A, Buckley DL, Parker GJM, editors. *Dynamic contrast-enhanced magnetic resonance imaging in oncology*. Berlin, Heidelberg: Springer; 2005. p 69-79.
20. Perles-Barbacaru AT, Lahrech H. A new magnetic resonance imaging method for mapping the cerebral blood volume fraction: The rapid steady-state T1 method. *J Cereb Blood Flow Metab* 2007;27:618-631.

21. Perles-Barbacaru AT, Berger F, Lahrech H. Quantitative rapid steady state T1 magnetic resonance imaging for cerebral blood volume mapping in mice: Lengthened measurement time window with intraperitoneal Gd-DOTA injection. *Magn Reson Med* 2013;69:1451-1456.
22. Perles-Barbacaru T-A, Procissi D, Demyanenko AV, Jacobs RE. Quantitative pharmacologic MRI in mice. *NMR Biomed* 2012;25:498-505.
23. Sarraf M, Perles-Barbacaru AT, Nissou MF, van der Sanden B, Berger F, Lahrech H. Rapid-steady-state-T1 signal modeling during contrast agent extravasation: Toward tumor blood volume quantification without requiring the arterial input function. *Magn Reson Med* 2015;73:1005-1014.
24. Moreno H, Hua F, Brown T, Small S. Longitudinal mapping of mouse cerebral blood volume with MRI. *NMR Biomed* 2006;19:535-543.
25. Bothe HW, Bodsch W, Hossmann KA. Relationship between specific gravity, water content, and serum protein extravasation in various types of vasogenic brain edema. *Acta Neuropathol* 1984;64:37-42.
26. Jivan A, Horsfield MA, Moody AR, Cherryman GR. Dynamic T1 measurement using snapshot-FLASH MRI. *J Magn Reson* 1997;127:65-72.
27. Shen Y, Goerner FL, Snyder C, et al. T1 relaxivities of gadolinium-based magnetic resonance contrast agents in human whole blood at 1.5, 3, and 7 T. *Invest Radiol* 2015;50:330-338.
28. Elst LV, Raynaud J-S, Vives V, et al. Comparative relaxivities and efficacies of Gadolinium-based commercial contrast agents. Proceedings of the 21st Annual Meeting of ISMRM, Salt Lake City, UT, USA. 2013. (abstract 0746).
29. Vérant P, Serduc R, Van Der Sanden B, Rémy C, Vial J-C. A direct method for measuring mouse capillary cortical blood volume using multiphoton laser scanning microscopy. *J Cereb Blood Flow Metab* 2007;27:1072-1081.
30. Chowdhury EA, Alqahtani F, Bhattacharya R, Mehvar R, Bickel U. Simultaneous UPLC-MS/MS analysis of two stable isotope labeled versions of sucrose in mouse plasma and brain samples as markers of blood-brain barrier permeability and brain vascular space. *J Chromatogr B Analyt Technol Biomed Life Sci* 2018;1073:19-26.
31. Kuo Y-T, Herlihy AH, So P-W, Bhakoo KK, Bell JD. In vivo measurements of T1 relaxation times in mouse brain associated with different modes of systemic administration of manganese chloride. *J Magn Reson Imaging* 2005;21:334-339.
32. Nair AB, Jacob S. A simple practice guide for dose conversion between animals and human. *J Basic Clin Pharm* 2016;7:27-31.
33. Huang S, Farrar CT, Dai G, et al. Dynamic monitoring of blood-brain barrier integrity using water exchange index (WEI) during mannitol and CO2 challenges in mouse brain. *NMR Biomed* 2013;26:376-385.
34. Weed LH. The absorption of cerebrospinal fluid into the venous system. *Am J Anat* 1923;31:191-221.
35. Kozerke S, Tsao J. Reduced data acquisition methods in cardiac imaging. *Top Magn Reson Imaging* 2004;15:161-168.
36. Koh TS, Shi W, Thng CH, Kwek JW, Bisdas S, Khoo JBK. Interpretation and applicability of empirical tissue enhancement metrics in dynamic contrast-enhanced MRI based on a multiple pathway model. *Phys Med Biol* 2012;57:N279-N294.
37. Deruelle T, Kober F, Perles-Barbacaru A, et al. A multicenter preclinical MRI study: Definition of rat brain relaxometry reference maps. *Front Neuroinform* 2020;14:22.
38. Koutcher JA, Burt CT, Lauffer RB, Brady TJ. Contrast agents and spectroscopic probes in NMR. *J Nucl Med* 1984;25:506-513.